NASA/TP-2000-209030

Thermoelastic Analysis of Hyper-X Camera Windows Suddenly Exposed to Mach 7 Stagnation Aerothermal Shock

William L. Ko and Leslie Gong
NASA Dryden Flight Research Center
Edwards, California

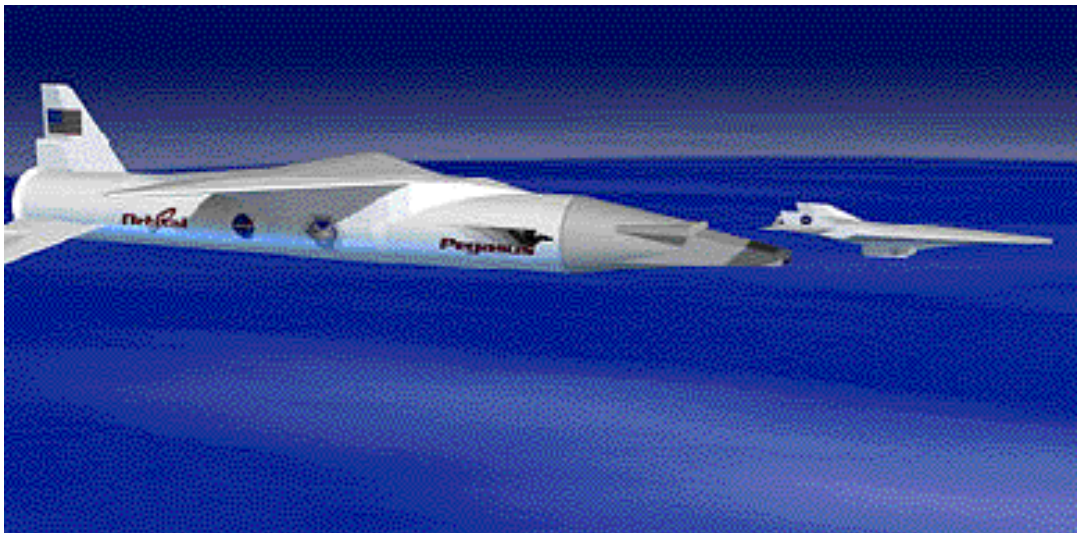

September 2000

The NASA STI Program Office…in Profile

Since its founding, NASA has been dedicated to the advancement of aeronautics and space science. The NASA Scientific and Technical Information (STI) Program Office plays a key part in helping NASA maintain this important role.

The NASA STI Program Office is operated by Langley Research Center, the lead center for NASA's scientific and technical information. The NASA STI Program Office provides access to the NASA STI Database, the largest collection of aeronautical and space science STI in the world. The Program Office is also NASA's institutional mechanism for disseminating the results of its research and development activities. These results are published by NASA in the NASA STI Report Series, which includes the following report types:

- TECHNICAL PUBLICATION. Reports of completed research or a major significant phase of research that present the results of NASA programs and include extensive data or theoretical analysis. Includes compilations of significant scientific and technical data and information deemed to be of continuing reference value. NASA's counterpart of peer-reviewed formal professional papers but has less stringent limitations on manuscript length and extent of graphic presentations.

- TECHNICAL MEMORANDUM. Scientific and technical findings that are preliminary or of specialized interest, e.g., quick release reports, working papers, and bibliographies that contain minimal annotation. Does not contain extensive analysis.

- CONTRACTOR REPORT. Scientific and technical findings by NASA-sponsored contractors and grantees.

- CONFERENCE PUBLICATION. Collected papers from scientific and technical conferences, symposia, seminars, or other meetings sponsored or cosponsored by NASA.

- SPECIAL PUBLICATION. Scientific, technical, or historical information from NASA programs, projects, and mission, often concerned with subjects having substantial public interest.

- TECHNICAL TRANSLATION. English-language translations of foreign scientific and technical material pertinent to NASA's mission.

Specialized services that complement the STI Program Office's diverse offerings include creating custom thesauri, building customized databases, organizing and publishing research results…even providing videos.

For more information about the NASA STI Program Office, see the following:

- Access the NASA STI Program Home Page at ***http://www.sti.nasa.gov***

- E-mail your question via the Internet to help@sti.nasa.gov

- Fax your question to the NASA Access Help Desk at (301) 621-0134

- Telephone the NASA Access Help Desk at (301) 621-0390

- Write to:
  NASA Access Help Desk
  NASA Center for AeroSpace Information
  7121 Standard Drive
  Hanover, MD 21076-1320

NASA/TP-2000-209030

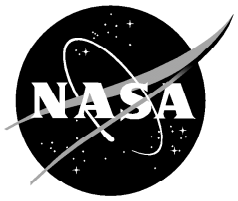

Thermoelastic Analysis of Hyper-X Camera Windows Suddenly Exposed to Mach 7 Stagnation Aerothermal Shock

William L. Ko and Leslie Gong
NASA Dryden Flight Research Center
Edwards, California

National Aeronautics and
Space Administration

Dryden Flight Research Center
Edwards, California 93523-0273

September 2000

ABSTRACT

To visually record the initial free flight event of the Hyper-X research flight vehicle immediately after separation from the Pegasus® booster rocket, a video camera was mounted on the bulkhead of the adapter through which Hyper-X rides on Pegasus. The video camera was shielded by a protecting camera window made of heat-resistant quartz material. When Hyper-X separates from Pegasus, this camera window will be suddenly exposed to Mach 7 stagnation thermal shock and dynamic pressure loading (aerothermal loading). To examine the structural integrity, thermoelastic analysis was performed, and the stress distributions in the camera windows were calculated. The critical stress point where the tensile stress reaches a maximum value for each camera window was identified, and the maximum tensile stress level at that critical point was found to be considerably lower than the tensile failure stress of the camera window material.

NOMENCLATURE

A_i	elementary surface area associated with radial location of node i, in^2
a	radius of circular camera window, in.
CTE	classical theory of elasticity
E	Young's modulus, lb/in^2
G	shear modulus, lb/in^2
h	thickness of camera window, in.
JLOC	joint location
Q_i	nodal force at r_i, lb
Q_o	nodal force at camera window center, lb
q	dynamic pressure, lb/ft^2
r, θ, z	cylindrical coordinate system
r_i	radial location of node i, in.
r_m	radial location where radial stress (σ_r) or tangential stress (σ_θ) reaches its maximum tensile value, in.
Δr	radial length of any element, in.
SPAR	Structural Performance and Resizing (finite-element computer program)
S61	pentahedron element or wedge element (six nodes)
S81	hexahedron element or brick element (eight nodes)
T	temperature, $^\circ$R or $^\circ$F
t	time counted from the instance Hyper-X separates from Pegasus booster rocket, sec

w	deflection of camera window at any radial location, in.
α	coefficient of thermal expansion, in./in.-˚F
δ	camera window center deflection, in.
ρ	density, lb/in^3
σ_C	compressive failure stress, lb/in^2
σ_r	radial stress, lb/in^2
$(\sigma_r)_{max}$	maximum value of σ_r, lb/in^2
σ_T	tensile failure stress, lb/in^2
σ_θ	tangential stress, lb/in^2
$(\sigma_\theta)_{max}$	maximum value of σ_θ, lb/in^2
v	Poisson's ratio

INTRODUCTION

Hyper-X (designated X-43) is a new hypersonic flight research vehicle (12 ft long, 5 ft span, 3,000 lb weight), designed to be flown in the Mach 7–10 range (fig. 1). The Hyper-X carries a scramjet (supersonic-combustion ramjet) engine using hydrogen as fuel and inlet air as oxidizer (without carrying oxidizer on board). The scramjet engine is a ramjet engine in which the airflow through the whole engine remains supersonic. Figure 2 shows the flight trajectory of Hyper-X. Hyper-X rides on a Pegasus® winged booster rocket, which is carried under the wing of the B-52 aircraft to a launch altitude of 17,000 ft for a Mach 7 mission or to 43,000 ft for a Mach 10 mission. After air launching from the B-52, the Pegasus accelerates and ascends to approximately 100,000 ft altitude, reaching the test velocity of Mach 7 or 10. After separation from the booster rocket, the cowl door of the scramjet opens to test the scramjet engine. After the cowl door is opened, fuel is injected, ignited, and burned for about 8 sec. The entire event from the opening of the cowl door to closing the cowl door takes 34 sec.

On the first Mach 7 mission, a video camera is to be used to visually record the staged separation (fig. 1). The camera is to be mounted on the bulkhead of the adapter used for the Hyper-X to ride on the Pegasus. The camera is to be housed inside a unit protected by a circular-disk-shaped quartz camera window made of fused silica (fig. 3). At booster separation (fig. 1), the camera window is to be exposed suddenly to Mach 7 aerothermal loading (i.e., stagnation heating and dynamic pressure loading). The interior of the camera window, however, initially will remain unheated. Such sudden surface heating is called thermal shock.

The severe temperature gradient across the camera window depth resulting from thermal shock induces compressive stresses in the heated zone and tensile stresses in the cooler interior zone. These stresses cause the camera window to bend outwardly (bulging deformation) if it is allowed to expand and bend freely. The dynamic pressure, on the other hand, tends to bend the window inwardly (caving deformation), inducing compression on the heated side and tension on the cool side. For brittle materials like the camera window, which has very low tensile strength, the induced tensile stresses raise serious

concerns about the structural integrity of the camera window. Increasing tensile stresses could crack the camera window, resulting in interference with the camera line-of-sight.

This report presents thermoelastic analysis results of the Hyper-X camera window subjected to Mach 7 thermal shock and dynamic pressure, and characterizes the thermoelastic performance of the camera window.

DESCRIPTION OF PROBLEM

The Hyper-X camera window is a circular disk with a radius $a = 2.52$ in. and a thickness h of either 0.25 or 0.50 in. (fig. 4). The disk is made of fused silica-Corning 7940 brittle material. The camera window disk is to be simply supported at its circumference and be subjected to Mach 7 stagnation thermal shock T and dynamic pressure q on its entire outer surface. The problem is to perform thermoelastic analysis of the camera window subjected to the said dual loading, and to calculate stress distributions in the camera window to predict the survivability of the camera window under Mach 7 aerothermal shock.

THERMAL RESPONSE

Figures 5 and 6 show temperature time histories calculated from transient heat transfer analysis for different thickness locations of camera windows of both thicknesses (provided by the camera window designer). The time t is counted from the instant Hyper-X is separated from the Pegasus booster rocket. Figures 7 and 8 are plots of the temperature profiles along the depth of the window at different time steps. Table 1 lists the temperature differences between the heated and cool sides at different times.

Table 1. Temperature differences between heated and cool sides.

ΔT, °F							
	t, sec						
h, in.	1	2	4	8	12	16	20
0.25	350	450	580	650*	650*	630	580
0.50	350	450	590	740	830	900	930*

* Maximum ΔT

As will be seen later, the highest value of ΔT does not necessarily induce the highest tensile stresses.

FINITE-ELEMENT ANALYSIS

The Structural Performance and Resizing (SPAR) finite-element computer program (ref. 1) was used in the linear uncoupled thermoelastic analysis and linear elastic analysis of the Hyper-X camera window.

Finite-Element Modeling

Because of axisymmetry, a small pie-shaped segment (θ degree sector) of the camera window disk was modeled (fig. 4). The sector angle θ was chosen to be 6 degrees for maintaining proper element shapes without excess distortion. Figures 9 and 10 show the two finite-element models generated for the pie-segments of the camera windows with thicknesses of 0.25 and 0.50 in., respectively. The joint locations (JLOC) are equally spaced in both the radial and thickness directions. Each model has only one layer of elements in the θ-direction. There are twenty elements in the radial direction and 10 elements in the thickness direction. The disk central region (tip of pie) is modeled with S61 elements (pentahedron or wedge elements), and the rest of the pie segment with S81 elements (hexahedron or brick elements). The sizes of the two finite element models are identical, as listed in table 2.

Table 2. Sizes of finite-element models for 6 degree pie-shaped segment of the Hyper-X camera window.

h, in.	JLOC	S61 elements	S81 elements
0.25	451	10	190
0.50	451	10	190

Material Properties

Table 3 lists the material properties of the fused silica-Corning 7940 used for the Hyper-X camera window.

Table 3. Material properties of camera window (fused silica-Corning 7940).

E	$= 10.5874 \times 10^6$ lb/in^2
G	$= 4.4960 \times 10^6$ lb/in^2
ν	$= 0.17$
σ_T	$= 7{,}251$ lb/in^2
σ_C	$= 159{,}536$ lb/in^2
ρ	$= 0.0795$ lb/in^3
α	$= 0.3056 \times 10^{-6}$ in./in.-°F

Note: Corning 7940 material has a very low coefficient of thermal expansion α and very low tensile failure stress σ_T.

Constraints

The pie-shaped model is constrained to have no tangential displacements and zero tangential slopes, but can move freely in both radial and thickness directions. The lower outermost nodes (camera window disk lower outer boundary) are simply supported. However, the support points move freely only in the radial direction (free expansion to minimize stress buildup). At the camera window center, only the motion in the thickness direction is allowed, and the slopes in both radial and tangential directions are set to zero.

Applied Loads

For the thermal loading, temperature distributions are assumed to be independent of r and θ coordinates, but are functions of z-coordinates. At each time step t, a temperature distribution curve (figs. 7, 8) associated with that time step was used at any (r, θ) location to generate nodal temperatures for nodes in the thickness direction.

For the pressure loading, dynamic pressure q = 1,002 lb/ft^2 was used. This value is the dynamic pressure at Mach 7 at the time that Hyper-X separates from the Pegasus booster.

Let A_i be the elementary surface area at radial location r_i, defined as

$$A_i = \left[\pi\left(r_i + \frac{\Delta r}{2}\right)^2 - \pi\left(r_i + \frac{\Delta r}{2}\right)^2\right]\left(\frac{\theta}{360}\right) = 2\pi r_i \, \Delta r \left(\frac{\theta}{360}\right) \tag{1}$$

where Δr is the radial length of A_i (or radial length of any finite element). The surface force $A_i q$ acting on A_i as a result of dynamic pressure q, is equally shared by two surface nodes at r_i. Thus, the nodal force Q_i to be applied at each surface node at r_i (except for disk center node) will be

$$Q_i = \frac{1}{2} A_i q \tag{2}$$

At the radial outer boundary where $r_i = a$, the elementary surface area A_i takes on the following form:

$$A_i = \left[\pi a^2 - \pi\left(a - \frac{\Delta r}{2}\right)^2\right]\left(\frac{\theta}{360}\right) \approx \pi a \Delta r \left(\frac{\theta}{360}\right) \tag{3}$$

Finally, the nodal force Q_o to be applied at the camera window center node is calculated from

$$Q_o = \pi q \left(\frac{\Delta r}{2}\right)^2 \left(\frac{\theta}{360}\right) \tag{4}$$

Solutions for the dynamic pressure loading case may be calculated from the classical theory of elasticity (CTE). However, finite-element solutions for this case are obtained to check the finite-element solution accuracy in light of CTE solutions, and therefore, to gain confidence in the adequacy of the finite-element modeling.

CLASSICAL THEORY

For a circular plate (for example, a camera window) under uniform surface pressure q on one side, the CTE, neglecting transverse shear effect, gives the following plate deflection $w(r)$ at any radial location (refs. 2, 3):

$$w(r) = \frac{3qa^4}{16Eh^3}(1-\nu)(5+\nu)\left[1-\left(\frac{1+\nu}{5+\nu}\right)\frac{r^2}{a^2}\right]\left(1-\frac{r^2}{a^2}\right) \tag{5}$$

At the center of the disk $(r = 0)$, $w(0)$ reaches a maximum; namely,

$$w(0) = \delta = \frac{3qa^4}{16Eh^3}(1-\nu)(5+\nu) \tag{6}$$

The stresses $\{\sigma_r(r,z), \sigma_\theta(r,z)\}$ induced at any radial location and depth reach their respective "local" tensile maximums $\{\sigma_r(r,0), \sigma_\theta(r,0)\}$ at $z = 0$ (inner cool surface). Those stresses $\{\sigma_r(r,0), \sigma_\theta(r,0)\}$ are given by the following (ref. 2):

$$\sigma_r(r,0) = \frac{3qa^2}{8h^2}(3+\nu)\left(1-\frac{r^2}{a^2}\right) \tag{7}$$

$$\sigma_\theta(r,0) = \frac{3qa^2}{8h^2}(3+\nu)\left[1-\left(\frac{1+3\nu}{3+\nu}\right)\frac{r^2}{a^2}\right] \tag{8}$$

At the disk center ($r = 0$), both σ_r and σ_θ reach the same maximum value of

$$\sigma_r(0,0) = \sigma_\theta(0,0) = \frac{3qa^2}{8h^2}(3+\nu) \tag{9}$$

As will be seen later, the displacements and stresses calculated from the CTE are amazingly close to the SPAR finite-element solutions.

RESULTS

The following sections present the results of thermoelastic analysis of the Hyper-X camera windows. Thermal loading results include thermal deformations and thermal stresses. Dynamic pressure loading includes mechanical deformations and mechanical stresses. The combined case includes results for total deformations and total stresses.

Thermal Loading

Thermal Deformations

Figures 11 and 12, respectively, show the deformed shapes of the h = 0.25 in. model and h = 0.50 in. model under Mach 7 heating. The displacements in the figures are highly magnified for easy visualization. Table 4 lists the camera window center deflections δ (figs. 11 and 12) calculated for the two models at different time steps, with peak values indicated with asterisks. The initial time $t = 0$ corresponds to the time when Hyper-X separates from the Pegasus.

Table 4. Camera window center deflections δ resulting from heating only.

δ, in. $\times 10^{-3}$							
	t, sec						
h, in.	1	2	4	8	12	16	20
0.25	0.695	1.170	1.760	2.230*	2.220	2.170	2.080
0.50	0.283	0.416	0.679	0.968	1.170	1.340	1.460*

* Peak value

Figure 13 is a plot of the data shown in table 4. For the 0.25-in.-thick camera window, the center deflection δ increases with increasing time and reaches a maximum value of $\delta = 2.230 \times 10^{-3}$ in. at t = 8 sec (indicated with arrow down), and then decreases slightly as the time advances. For the 0.50-in.-thick camera window, δ increases monotonically with advancing time and reaches a maximum value of 1.460×10^{-3} in. (indicated with arrow down) at the end of the time range (t = 20 sec).

Thermal Stresses

Figure 14 shows the radial distribution of both radial and tangential tensile stresses $\{\sigma_r, \sigma_\theta\}$ on the z/h = 0.65 plane measured from the cool inner surface. This z/h = 0.65 plane is where the values of $\{\sigma_r, \sigma_\theta\}$ reach their respective local tensile maximum. In the radial stress plots (fig. 14), $\{\sigma_r, \sigma_\theta\}$ reach their respective maximum values $\{(\sigma_r)_{max}, (\sigma_\theta)_{max}\}$ at slightly different radial locations $r = r_m$ near the free boundary. For the h = 0.25 in. case, $(\sigma_r)_{\max}$ occurs at r_m/a = 0.875 cross section, and $(\sigma_\theta)_{max}$ at r_m/a = 0.925 cross section. For the h = 0.25 in. case, $(\sigma_r)_{max}$ is at r_m/a = 0.775 cross section, and $(\sigma_\theta)_{max}$ at r_m/a = 0.875 cross section. Note that the maximum values $\{(\sigma_r)_{max}, (\sigma_\theta)_{max}\}$ are only about 3 percent higher than the values of $\{\sigma_r, \sigma_\theta\}$ in the uniform flat regions of the plots. The extreme proximity of the two stresses (except the free boundary at $r = a$) implies that the camera window is practically under an equal biaxial stress field. At the camera window center (r = 0), the radial and tangential stresses become identical because of a pure biaxial stress field.

Figure 15 shows the depth-wise distributions of radial and tangential stresses $\{\sigma_r, \sigma_\theta\}$ at $r = r_m$ cross section (fig. 14) for the two thicknesses of camera windows. The high compression (negative sign) near the heated surface is the result of the resisted thermal expansion, and moderate compression near the cool surface is induced by the thermal bending of the camera window. At the camera window center ($r = 0$), the two curves of $\{\sigma_r, \sigma_\theta\}$ for each case of h in figure 15 will collapse into a single curve because of the pure biaxial stress field (fig. 14).

Tables 5 and 6, respectively, show the maximum tensile radial and tangential stresses $\{(\sigma_r)_{max}, (\sigma_\theta)_{max}\}$ induced in the two types of camera windows at different time steps.

Table 5. Maximum radial tensile thermal stresses $(\sigma_r)_{max}$ induced in camera window.

$(\sigma_r)_{max}$, lb/in^2							
	t, sec						
h, in.	1	2	4	8	12	16	20
0.25	209.1	235.3	236.7*	225.3	200.8	163.5	147.4
0.50	203.3	250.7	313.0	377.5	389.2*	362.4	355.8

* Peak value Note: Tensile failure stress $(\sigma_T) = 7{,}251$ lb/in^2

Table 6. Maximum tangential tensile thermal stresses $(\sigma_\theta)_{max}$ induced in camera window.

$(\sigma_\theta)_{max}$, lb/in^2							
	t, sec						
h, in.	1	2	4	8	12	16	20
0.25	207.6	233.8	235.7*	221.1	198.6	163.2	144.6
0.50	202.9	252.4	315.1	379.8	391.4*	364.4	357.6

* Peak value Note: Tensile failure stress $(\sigma_T) = 7{,}251$ lb/in^2

Figure 16 is a plot of the data shown in tables 5 and 6. For the 0.25-in.-thick camera window, $\{(\sigma_r)_{max}, (\sigma_\theta)_{max}\}$ reach their respective peak values at $t = 4$ sec after Hyper-X separation. For the 0.50-in.-thick camera window, $\{(\sigma_r)_{max}, (\sigma_\theta)_{max}\}$ reach their peak values at $t = 12$ sec after Hyper-X separation. The peak values of $\{(\sigma_r)_{max}, (\sigma_\theta)_{max}\}$ are well below the value of tensile failure stress $\sigma_T = 7,251$ lb/in^2 of the camera window material. These are only partial stresses and must be

combined with the corresponding mechanical stresses to find the total stresses (the principle of superposition holds for linear elasticity).

Dynamic Pressure Loading

Mechanical Deformations

Figures 17 and 18, respectively, show the deformed shapes of the $h = 0.25$ in. and $h = 0.50$ in. models under Mach 7 dynamic pressure $q = 1{,}002$ lb/ft^2. The camera windows deformed inward resulting from the surface dynamic pressure. Table 7 lists the amounts of displacement at the camera window centers calculated using the finite-element method and CTE (eq. (6)). The percentage differences between the SPAR and CTE solutions are also shown.

Table 7. Camera window center displacements resulting from dynamic pressure only.

	δ, in. $\times 10^{-3}$		
h, in.	SPAR	CTE	Solution difference, percent
0.25	–1.370	–1.365	0.366
0.50	–0.178	–0.171	4.094

The magnitudes of δ are slightly larger for the finite-element solutions because transverse shear effect was considered. The CTE solution neglected the transverse shear effect. The transverse shear effect is more conspicuous for the thick disk ($h = 0.50$ in.). Notice that the inward displacement of the $h = 0.50$-in. case is about 12.99 percent that of the $h = 0.25$-in. case because of double thickness. The CTE solution gives $(0.25/0.5)^3 \times 100 = 12.5$ percent (eq. (6)) because of neglecting the transverse shear effect. The percentage differences between the two solutions are quite small. The percentage solution difference for the $h = 0.50$-in. case is about 11 times that for the $h = 0.25$-in. case.

Mechanical Stresses

Figure 19 shows the radial distribution of local maximum radial and tangential tensile stresses at the inner cool surface ($z/h = 0$) calculated from both SPAR and CTE. The two types of solutions are amazingly close. This closeness implies that the present finite element modeling is adequate. The two stresses reached an identical maximum at the disk center. Unlike the heating case, the equal biaxial stress field exists only at the center of the camera window (eqs. (7), (8)).

Figure 20 shows the plots of the radial stresses (or tangential stresses; $\sigma_\theta(0, z) = \sigma_r(0, z)$) at the disk center as functions of depth z/h. Table 8 summarizes the maximum tensile stresses, located at the

cool side of the camera window center, calculated from both SPAR and CTE because of uniform pressure q, including the percent solution difference. The SPAR and CTE solutions are extremely close.

Table 8. Maximum tensile stresses at camera window; center cool side $(r = z = 0)$; dynamic pressure only.

	$\sigma_r(0, 0)\,[= \sigma_\theta(0, 0)]$, lb/in^2		
h, in.	SPAR	CTE	Solution difference, percent
0.25	840.90	840.46	0.0524
0.50	211.30	210.11	0.5664

Note: Tensile failure stress σ_T = 7,251 lb/in^2.

By doubling the disk thickness from 0.25 to 0.50 in., the maximum stress at the disk center is reduced to one-quarter (see eq. (9)). Like the mechanical displacement case, the percentage difference between the two types of stress solutions for the h = 0.50-in. case is about 11 times that for the h = 0.25-in. case.

Combined Case

Total Deformations

For the present linear thermoelastic analysis, the principle of superposition holds. Thus, the displacements at the camera window center caused by heating (table 4) and dynamic pressure loading (table 7) may be combined to give the total displacements δ, which table 9 summarizes.

Table 9. Total displacements at camera window center caused by T and q.

	δ, in. $\times 10^{-3}$							
	t, sec							
h, in.	0	1	2	4	8	12	16	20
0.25	–1.370	–0.675	–0.200	0.390	0.860*	0.850	0.800	0.710
0.50	–0.178	0.105	0.238	0.501	0.790	0.992	1.162	1.282*

* Peak value

The δ values at 0 sec are the result of dynamic pressure only, because heating has not yet started. Figure 21 is a plot of the data listed in table 9. Initially, the camera windows deformed inwardly as a result of dynamic pressure, but gradually deform outwardly as they are heated. For the 0.25-in.-thick window, δ reaches a maximum at 8 sec. For the 0.50-in.-thick window, δ increases monotonically with time during the initial 20-sec time period.

Total Stresses

By using the superposition principle allowed by linear elasticity, we superimposed the plots of stresses at camera window centers, resulting from heating, (not shown, but very similar to the plots of fig. 15) on the stress plots of figure 20, caused by dynamic pressure, to obtain the total stresses at the centers of camera windows. Figure 22 is a plot of the results. The compressive stresses at the outer surfaces of both camera windows caused by dynamic pressure are magnified through heating. The total compressive stresses at the camera window outer surfaces for both camera windows are very close. The peak total tensile stress shown by the curve for the 0.25-in.-thick window (fig. 22) is at 4 sec, and is less than the mechanical tensile stress resulting from dynamic pressure at 0 sec (fig. 20). However, the peak total tensile stress given by the curve for the 0.50-in.-thick window (fig. 22) is the true maximum tensile stress. Table 10 summarizes the total tensile stresses at different time steps and their *z*-locations.

Table 10. Total tensile stresses at camera window centers resulting from *T* and *q*.

h, in.	*t*, sec	$\sigma_r(0, z)$ [= $\sigma_\theta(0, z)$], lb/in^2	*z*/*h*	Percent of σ_T (= 7,251 lb/in^2)**
0.25	0	840.90*	0 (cool side)	11.60
0.25	4	528.35	0 (cool side)	7.29
0.50	0	211.30	0 (cool side)	2.91
0.50	12	336.85*	0.55 from cool side	4.65

* Maximum value
** Tensile failure stress

For the 0.25-in.-thick window, the maximum tensile stress is at the inner surface ($z/h = 0$), and occurs at 0 sec before thermal effect initiates. For the 0.50-in.-thick window, the maximum stress is mainly caused by thermal effect, and occurs at 12 sec, located at $z/h = 0.55$ measured from the cool side. It is seen that those maximum tensile stress values are well below the tensile failure stress σ_T = 7,251 lb/in^2 of the camera window material. Thus, camera windows of both thicknesses could perform well without failure under Mach 7 aerothermal loading.

CONCLUSIONS

Thermoelastic analysis was performed on the Hyper-X camera windows subjected to sudden Mach 7 aerothermal loading. The key results of the analysis are as follows:

1. Initially, the camera windows of both thickness deformed inwardly as a result of dynamic pressure, and then deformed outwardly as they were heated. The camera window center outward deflection reached a maximum at $t = 8$ sec for the 0.25-in.-thick camera window, but monotonically increased during the initial 20 sec for the 0.50-in.-thick camera window.
2. For the 0.25-in.-thick camera window, the maximum tensile stress was at $t = 0$ sec as a result of air load alone, and was at the inner surface. For the 0.50-in.-thick camera window, the maximum

tensile stress resulted from combined heating and air load, and occurred at t = 12 sec at location z/h = 0.55 measured from the cool inner surface.

3. The maximum total tensile stresses induced in the 0.25- and 0.50-in.-thick camera windows were, respectively, 11.60 percent (at t = 0 sec) and 4.65 percent (at t = 12 sec) of the tensile failure stress. Thus, the Hyper-X camera window will be able to perform well without failure under Mach 7 aerothermal shock.

4. Both heating and air-load induced compressive stresses at the outer surfaces of camera windows and the magnitudes for the two thickness cases were quite close.

Dryden Flight Research Center
National Aeronautics and Space Administration
Edwards, California, June 13, 2000

REFERENCES

1. Whetstone, W. D., *SPAR Structural Analysis System Reference Manual, System Level 13A, Vol. 1, Program Execution*, NASA CR-158970-1, December 1978.

2. Roark, Raymond J., *Formulas for Stress and Strain*, McGraw-Hill Book Co., Inc., New York, 1954, p. 194.

3. Timoshenko, S. and S. Woinowsky-Krieger, *Theory of Plates and Shells*, McGraw-Hill Book Co., Inc., New York, 1959, p. 57.

FIGURES

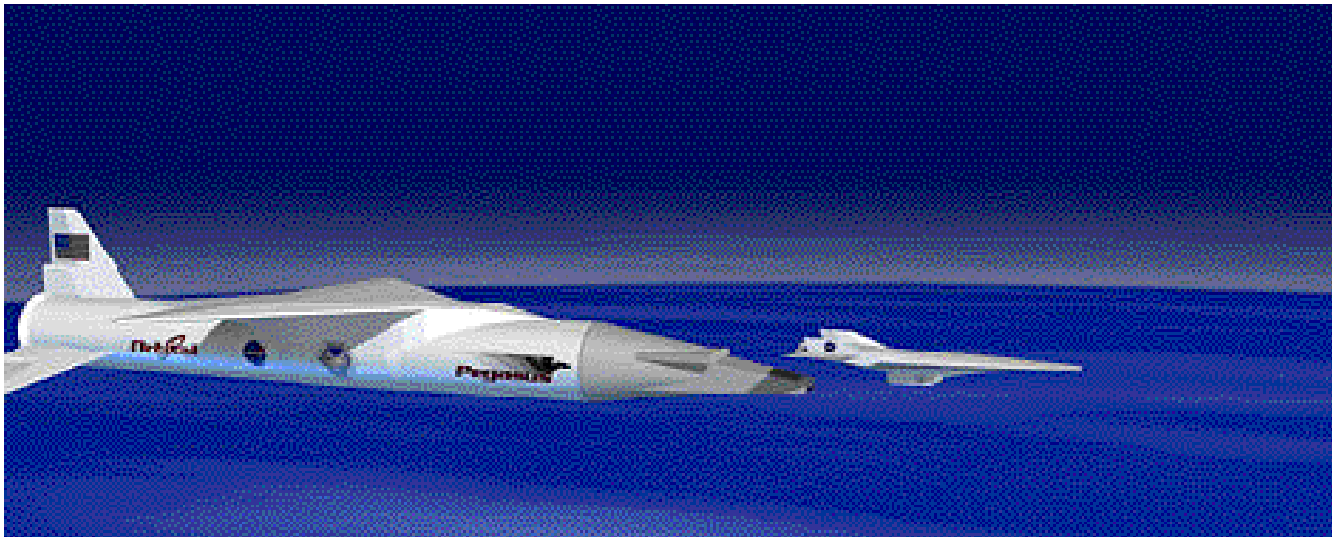

Figure 1. Artist's conception of separation of Hyper-X from Pegasus® booster rocket for experimental flight.

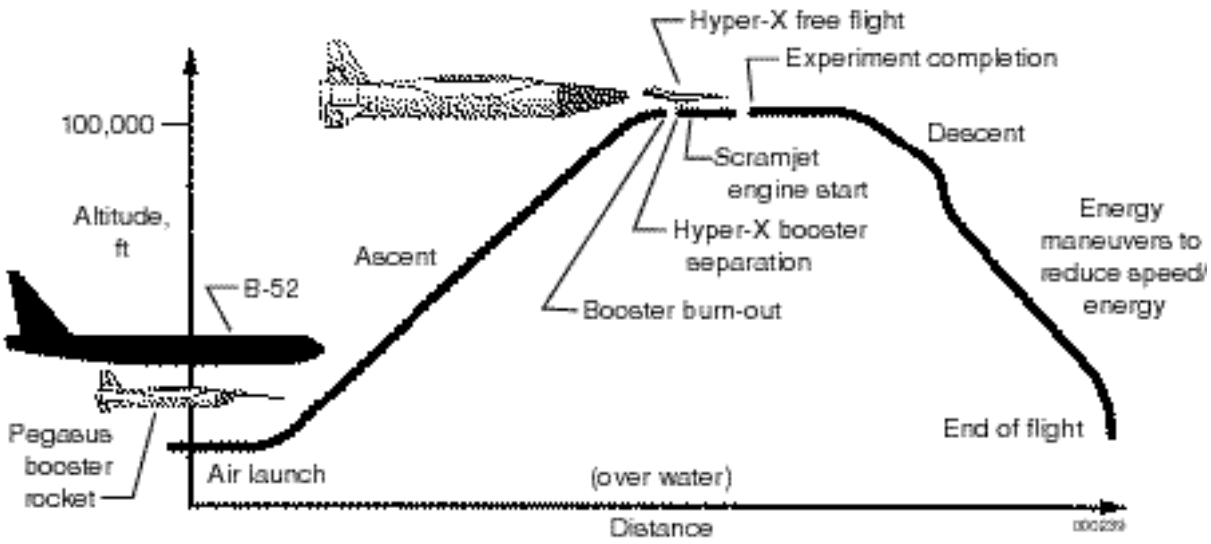

Figure 2. Hyper-X hypersonic flight research vehicle flight trajectory.

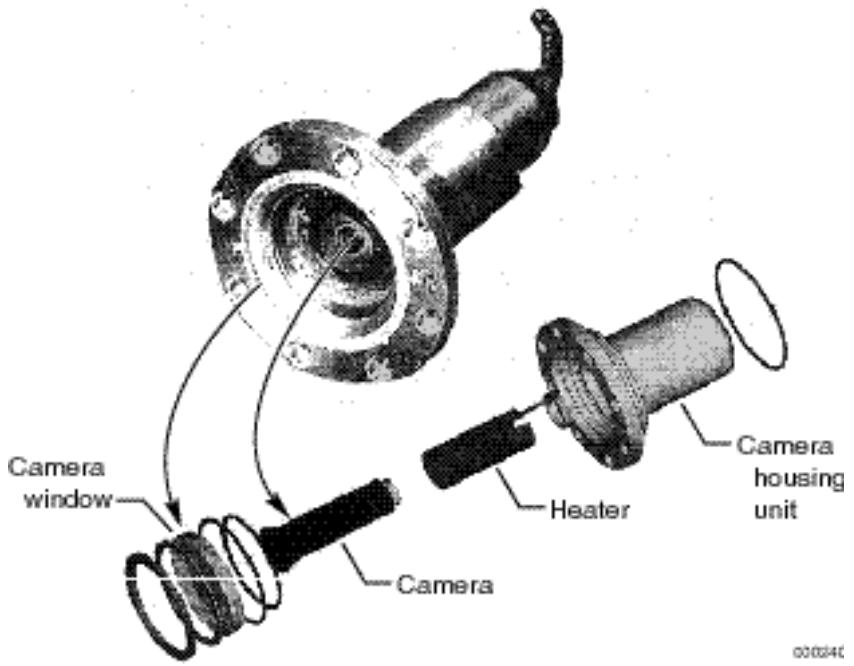

Figure 3. Camera system for recording the initial event of Hyper-X free flight.

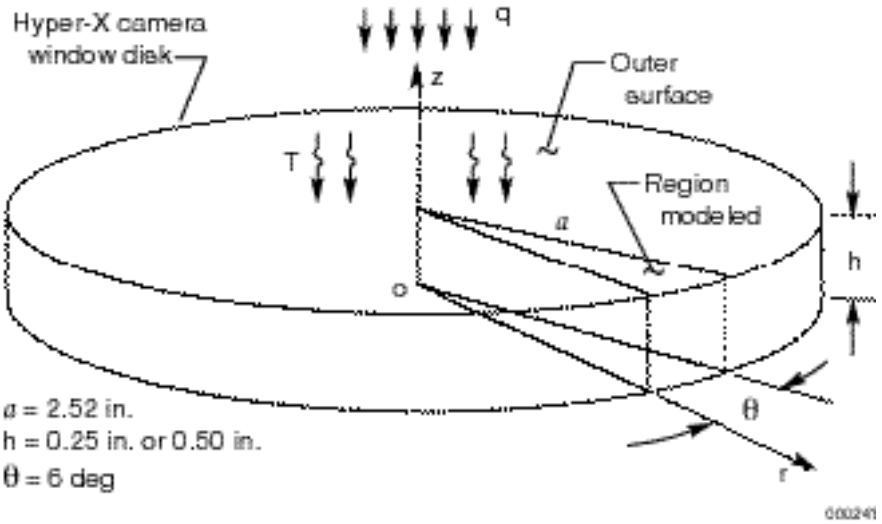

Figure 4. Hyper-X camera window disk subjected to thermal shock *T* and aerodynamic pressure *q* over the entire outer surface.

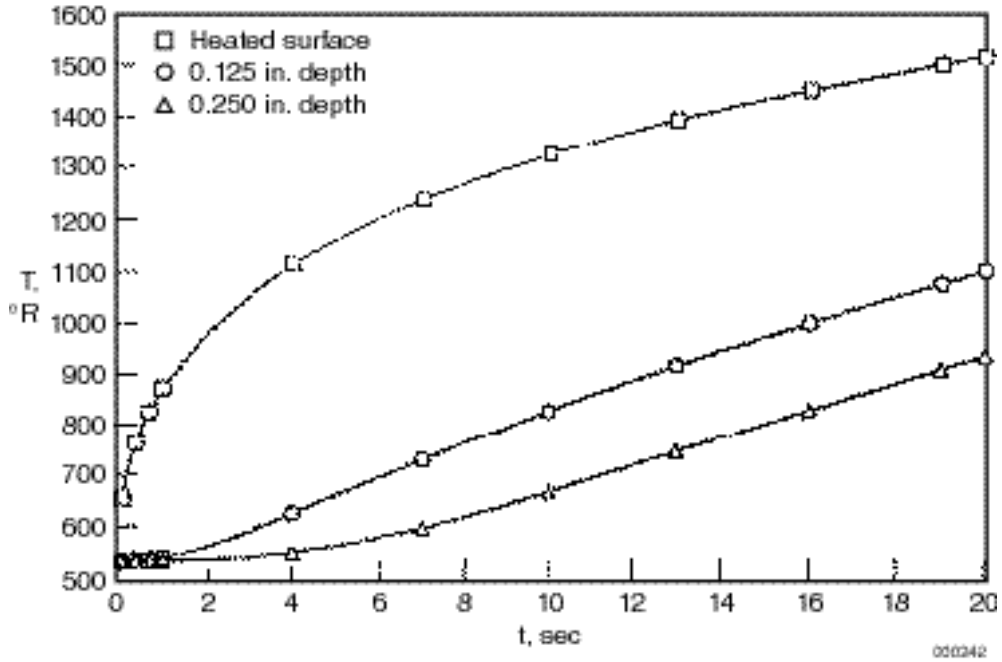

Figure 5. Temperature profile of camera window under Mach 7 heating; h = 0.25 in.

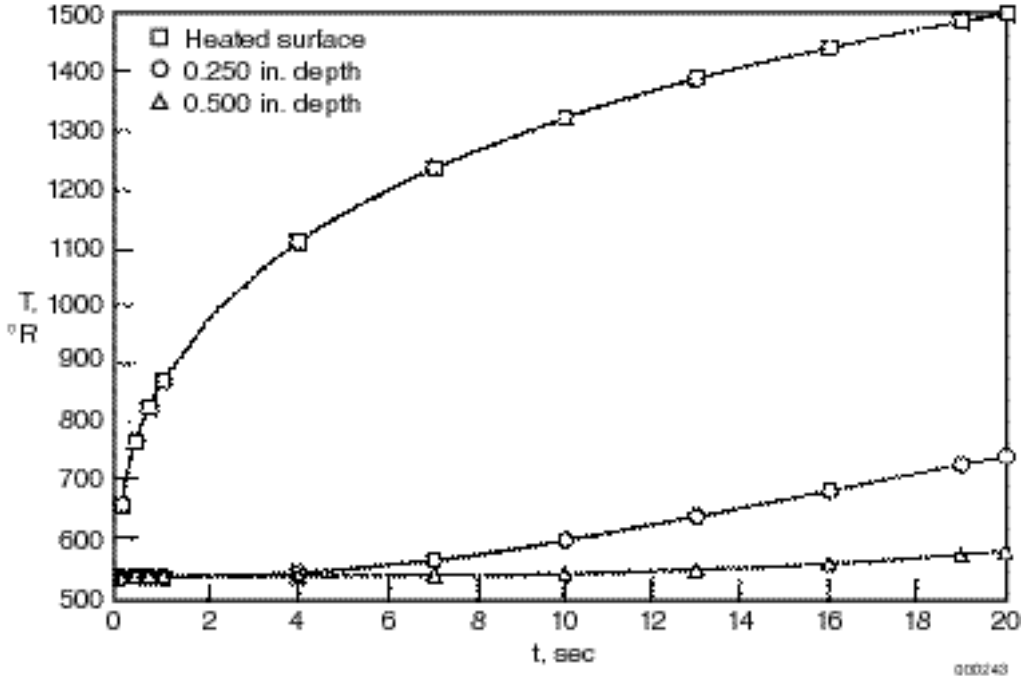

Figure 6. Temperature profile of camera window under Mach 7 heating; h = 0.50 in.

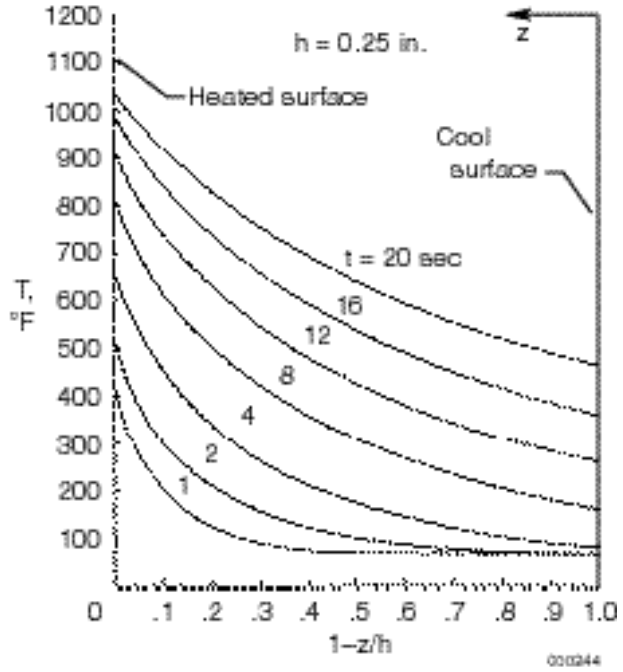

Figure 7. Temperature distributions through camera window depth at different time steps; Mach 7 heating; h = 0.25 in.

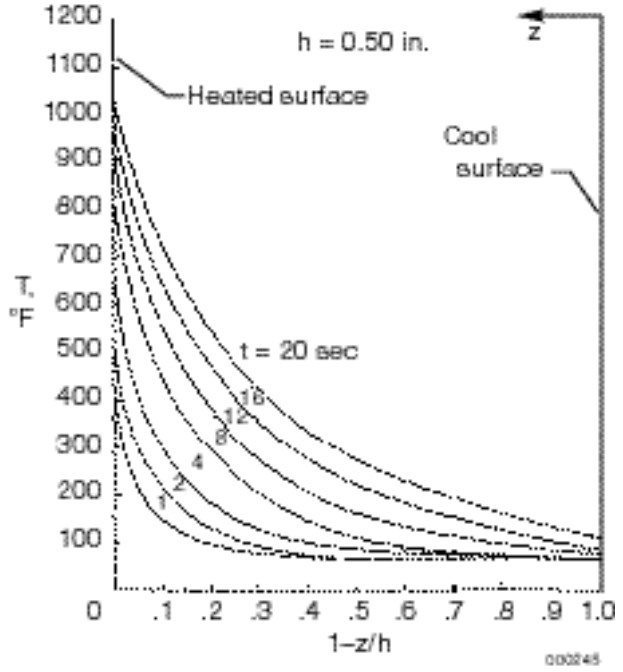

Figure 8. Temperature distributions through camera window depth at different time steps; Mach 7 heating; h = 0.50 in.

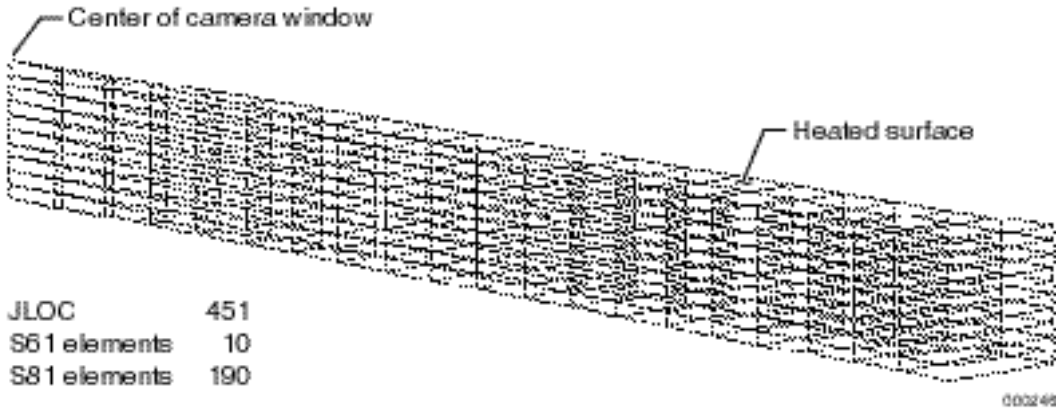

Figure 9. Finite-element model for a pie segment of camera window; h = 0.25 in.

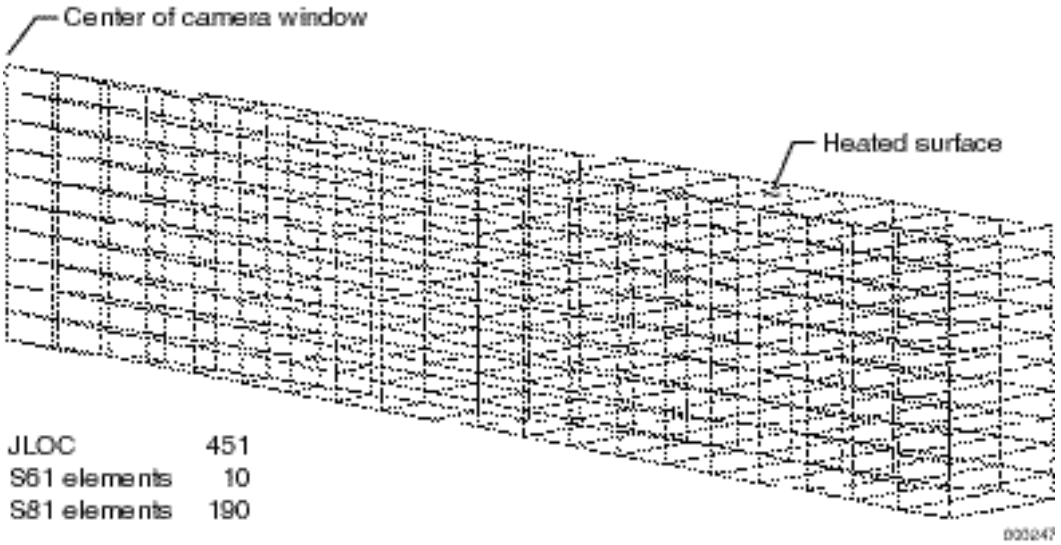

Figure 10. Finite-element model for a pie segment of camera window; h = 0.50 in.

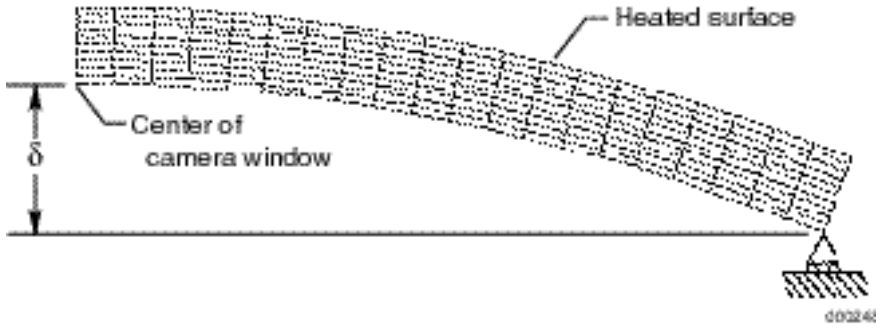

Figure 11. Deformed shape of camera window as a result of Mach 7 heating; h = 0.25 in.

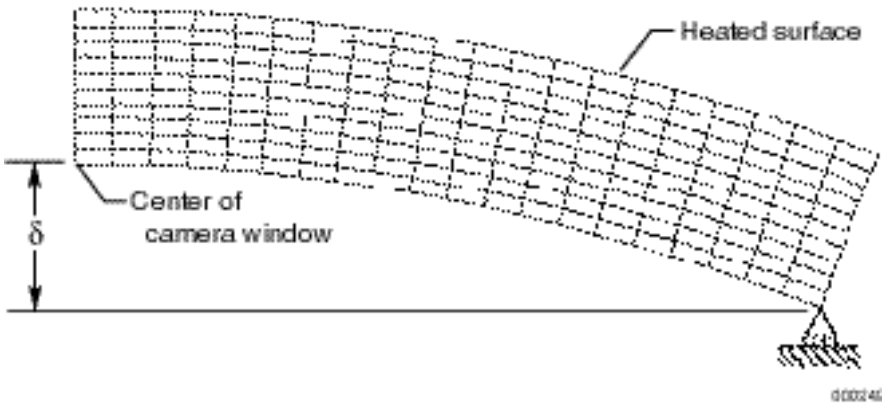

Figure 12. Deformed shape of camera window as a result of Mach 7 heating; h = 0.50 in.

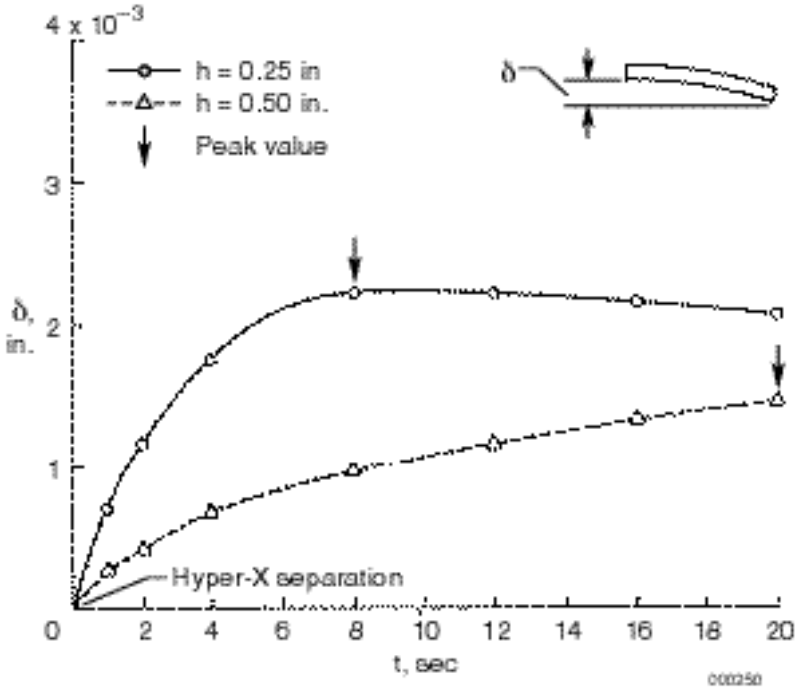

Figure 13. Plots of camera window center displacements δ as functions of time *t*; *t* = 0 is defined as the separation time of Hyper-X from Pegasus booster rocket; Mach 7 heating.

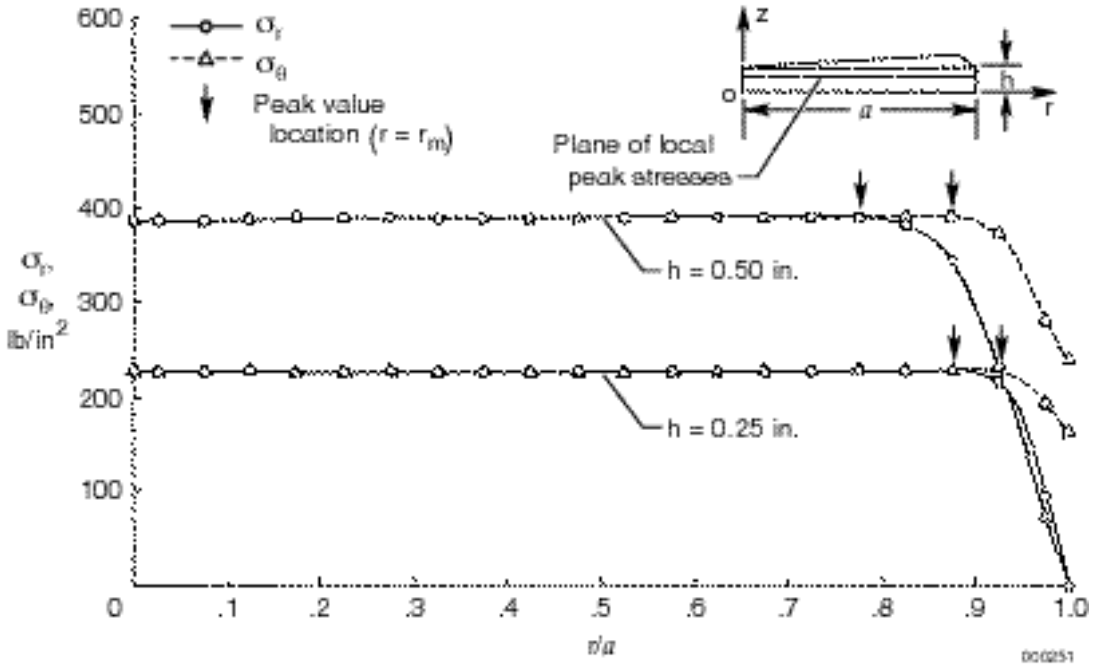

Figure 14. Radial distributions of local peak radial and tangential tensile stresses at depth *z*/*h* = 0.65 from cool side; Mach 7 heating.

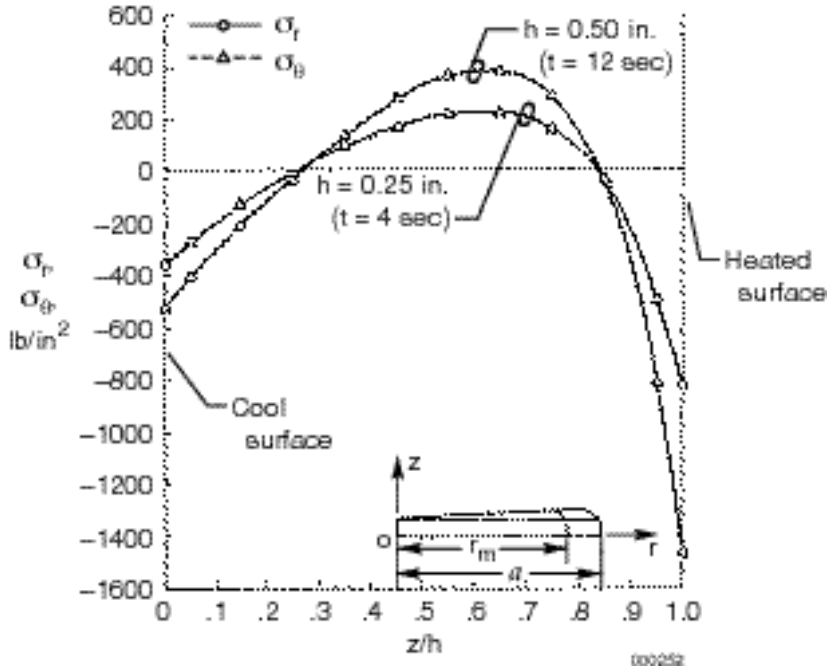

Figure 15. Plots of radial and tangential stresses $\{\sigma_r, \sigma_\theta\}$ as functions of depth *z*/*h*; σ_r at $r_m/a = 0.875$; σ_θ at $r_m/a = 0.925$; $t = 4$ sec for $h = 0.25$ in.; σ_r at $r_m/a = 0.775$; σ_θ at $r_m/a = 0.875$; $t = 12$ sec for $h = 0.50$ in.; Mach 7 heating.

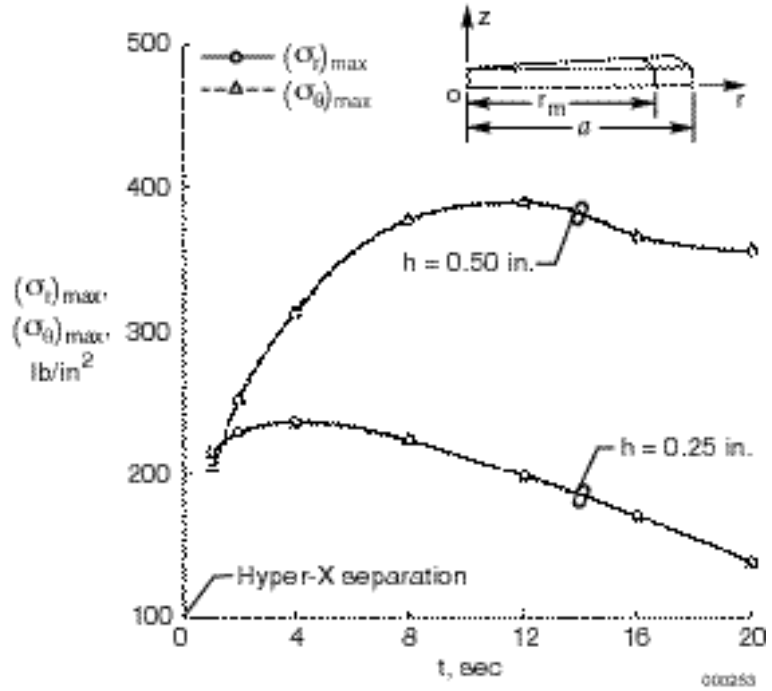

Figure 16. Plots of maximum radial and tangential tensile stresses $\{(\sigma_r)_{max}, (\sigma_\theta)_{max}\}$ at r_m cross section as functions of time *t*; $t = 0$ is defined as the separation time of Hyper-X from Pegasus booster rocket; Mach 7 heating.

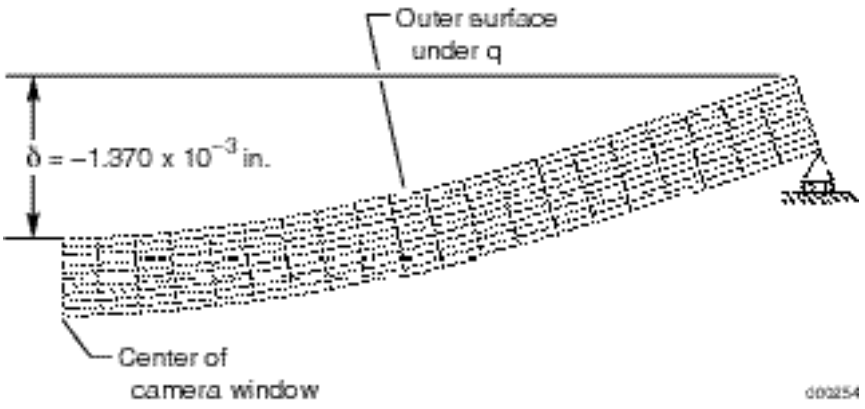

Figure 17. Deformed shape of camera window under Mach 7 dynamic pressure loading; q = 1,002 lb/ft^2; h = 0.25 in.

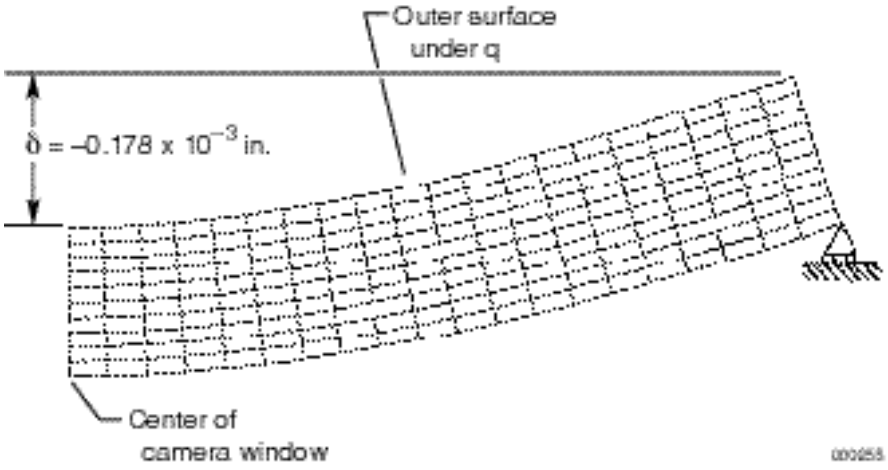

Figure 18. Deformed shape of camera window under Mach 7 dynamic pressure loading; q = 1,002 lb/ft^2; h = 0.50 in.

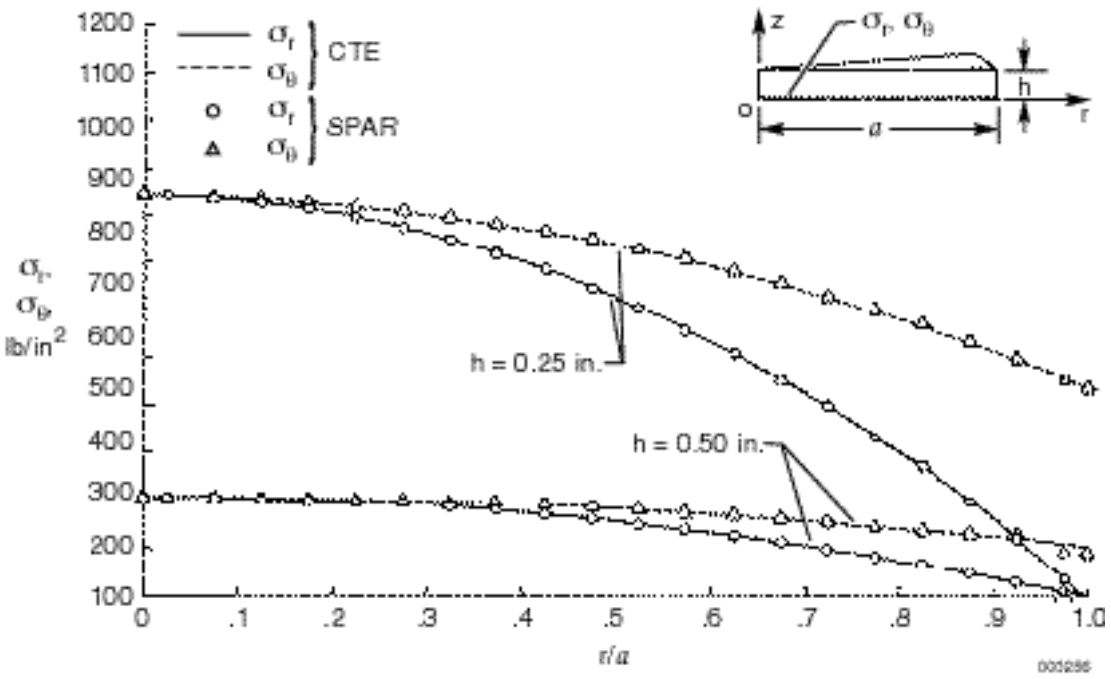

Figure 19. Radial distributions of radial and tangential tensile stresses $\{\sigma_r, \sigma_\theta\}$ at camera window cool-side boundary; Mach 7 aerodynamic pressure loading; q = 1,002 lb/ft^2.

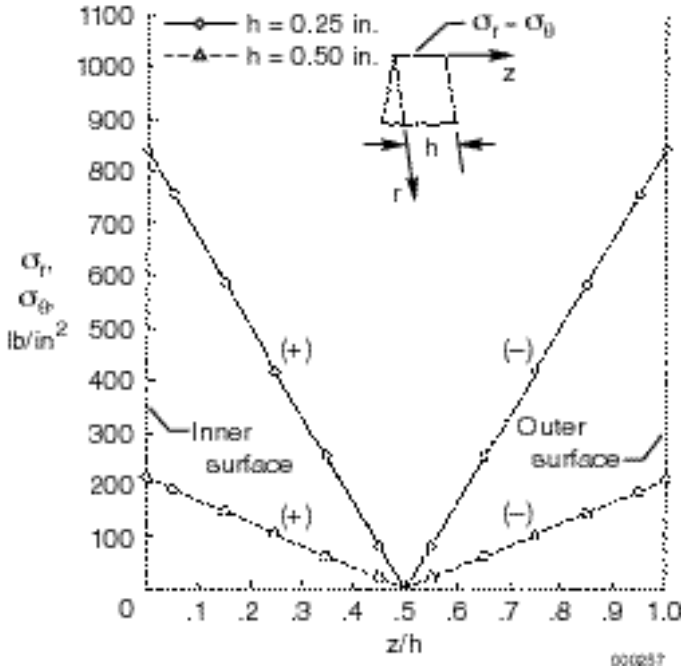

Figure 20. Plots of radial or tangential stress $\{\sigma_\theta(0, z) = \sigma_r(0, z)\}$ at camera window center (r = 0) as functions of depth z/h; Mach 7 dynamic pressure loading; q = 1,002 lb/ft^2.

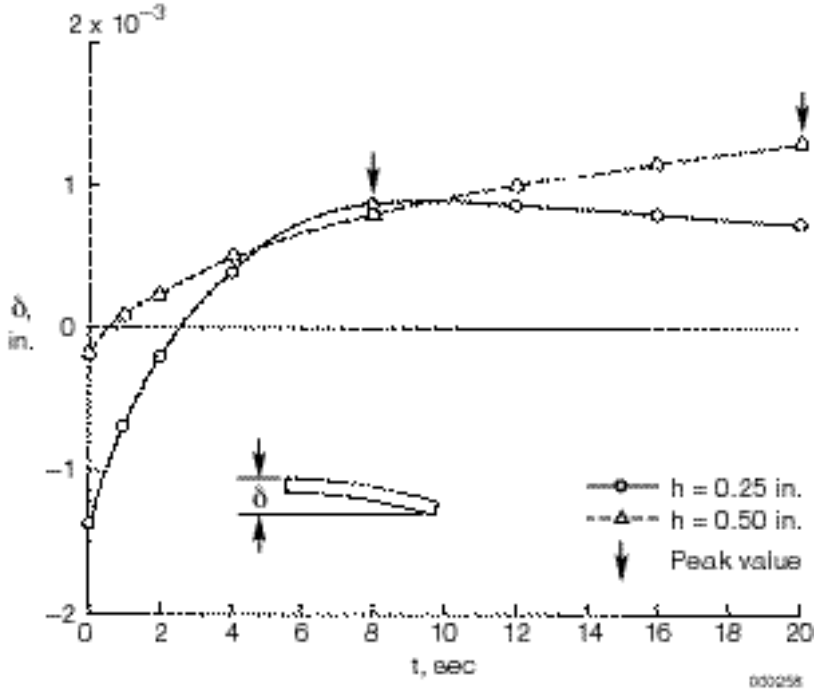

Figure 21. Plots of total camera window center displacements δ as functions of time t; $t = 0$ is defined as the separation time of Hyper-X from Pegasus booster rocket.

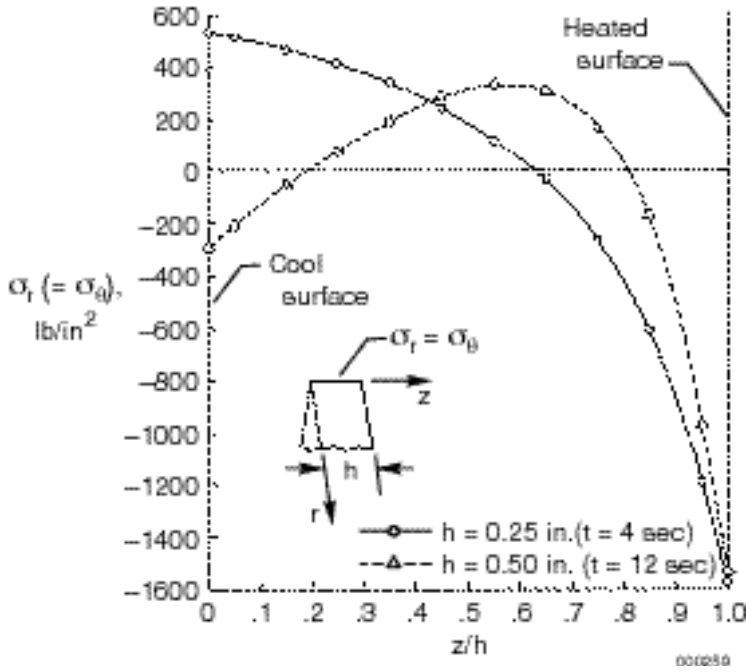

Figure 22. Plots of combined radial or tangential stress $\{\sigma_\theta(0, z) = \sigma_r(0, z)\}$ at camera window center ($r = 0$) as functions of depth z/h; thermal stress components at $t = 4$ sec for $h = 0.25$ in.; at $t = 12$ sec for $h = 0.50$ in.; mechanical stress components due to $q = 1{,}002$ lb/ft^2.

REPORT DOCUMENTATION PAGE

Form Approved
OMB No. 0704-0188

1. AGENCY USE ONLY (Leave blank)	2. REPORT DATE	3. REPORT TYPE AND DATES COVERED
	September 2000	Technical Publication

4. TITLE AND SUBTITLE

Thermoelastic Analysis of Hyper-X Camera Windows Suddenly Exposed to Mach 7 Stagnation Aerothermal Shock

5. FUNDING NUMBERS

WU 522-51-54-E8-50-00-X43

6. AUTHOR(S)

William L. Ko and Leslie Gong

7. PERFORMING ORGANIZATION NAME(S) AND ADDRESS(ES)

NASA Dryden Flight Research Center
P.O. Box 273
Edwards, California 93523-0273

8. PERFORMING ORGANIZATION REPORT NUMBER

H-2420

9. SPONSORING/MONITORING AGENCY NAME(S) AND ADDRESS(ES)

National Aeronautics and Space Administration
Washington, DC 20546-0001

10. SPONSORING/MONITORING AGENCY REPORT NUMBER

NASA/TP-2000-209030

11. SUPPLEMENTARY NOTES

12a. DISTRIBUTION/AVAILABILITY STATEMENT

Unclassified—Unlimited
Subject Category 39

This report is available at http://www.dfrc.nasa.gov/DTRS/

12b. DISTRIBUTION CODE

13. ABSTRACT (Maximum 200 words)

To visually record the initial free flight event of the Hyper-X research flight vehicle immediately after separation from the Pegasus® booster rocket, a video camera was mounted on the bulkhead of the adapter through which Hyper-X rides on Pegasus. The video camera was shielded by a protecting camera window made of heat-resistant quartz material. When Hyper-X separates from Pegasus, this camera window will be suddenly exposed to Mach 7 stagnation thermal shock and dynamic pressure loading (aerothermal loading). To examine the structural integrity, thermoelastic analysis was performed, and the stress distributions in the camera windows were calculated. The critical stress point where the tensile stress reaches a maximum value for each camera window was identified, and the maximum tensile stress level at that critical point was found to be considerably lower than the tensile failure stress of the camera window material.

14. SUBJECT TERMS

Circular disk, Dynamic pressure bending, Mach 7 heating, Mechanical stresses, Thermal shock, Thermal stresses.

15. NUMBER OF PAGES

29

16. PRICE CODE

A03

17. SECURITY CLASSIFICATION OF REPORT	18. SECURITY CLASSIFICATION OF THIS PAGE	19. SECURITY CLASSIFICATION OF ABSTRACT	20. LIMITATION OF ABSTRACT
Unclassified	Unclassified	Unclassified	Unlimited